

Machine learning-based moment closure model for the semiconductor Boltzmann equation with uncertainties

Juntao Huang · Liu Liu · Kunlun Qi ·
Jiayu Wan

the date of receipt and acceptance should be inserted later

Abstract In this paper, we propose a machine learning (ML)-based moment closure model for the linearized Boltzmann equation of semiconductor devices, addressing both the deterministic and stochastic settings. Our approach leverages neural networks to learn the spatial gradient of the unclosed highest-order moment, enabling effective training through natural output normalization. For the deterministic problem, to ensure global hyperbolicity and stability, we derive and apply the constraints that enforce symmetrizable hyperbolicity of the system. For the stochastic problem, we adopt the generalized polynomial chaos (gPC)-based stochastic Galerkin method to discretize the random variables, resulting in a system for which the approach in the deterministic case can be used similarly. Several numerical experiments will be shown to demonstrate the effectiveness and accuracy of our ML-based moment closure model for the linear semiconductor Boltzmann equation with (or without) uncertainties.

J. Huang

Department of Mathematics and Statistics, Texas Tech University, Lubbock, TX, 79409, USA. Research is partially supported by NSF DMS-2309655 and DOE DE-SC0023164.
E-mail: juntao.huang@ttu.edu

L. Liu

The Chinese University of Hong Kong, Hong Kong. L. Liu acknowledges the support by National Key R&D Program of China (2021YFA1001200), Ministry of Science and Technology in China, Early Career Scheme (24301021) and General Research Fund (14303022 & 14301423) funded by Research Grants Council of Hong Kong.
E-mail: lliu@math.cuhk.edu.hk

K. Qi

School of Mathematics, University of Minnesota - Twin Cities, Minneapolis, MN, 55455 USA.
E-mail: kqi@umn.edu

J. Wan

The Chinese University of Hong Kong, Hong Kong
E-mail: jiyuwan@cuhk.edu.hk

Keywords moment closure · linear Boltzmann equation · machine learning · uncertainty quantification

1 Introduction

Background: Kinetic equations have been widely used in many areas such as rarefied gas, plasma physics, astrophysics, semiconductor device modeling, and social and biological sciences [46, 60]. They describe the non-equilibrium dynamics of a system composed of a large number of particles and bridge atomistic and continuum models in the hierarchy of multiscale modeling. The Boltzmann-type equation, as one of the most representative models in kinetic theory, provides a power tool to describe molecular gas dynamics, radiative transfer, plasma physics, and polymer flow [3]. They have significant impacts in designing, optimization, control, and inverse problems. For example, it can be used in the design of semiconductor devices, topology optimization of gas flow channels, or risk management in quantitative finance [16]. Many of these applications often require finding unknown or optimal parameters in the Boltzmann-type equations or mean-field models [1, 7, 13, 15]. The linearized Boltzmann equation, particularly the semi-conductor Boltzmann equation in this work, has wide applications in semiconductor device modeling [4].

In addition, kinetic equations typically involve various sources of uncertainty, such as modeling errors, imprecise measurements, and uncertain initial conditions. As a result, addressing uncertainty quantification (UQ) becomes essential for evaluating, validating, and improving the underlying models, underscoring our project’s significance. In particular, the collision kernel or scattering cross-section in the Boltzmann equation governs the transition rates during particle collisions. Calculating this collision kernel from first principles is highly complex, and in practice, heuristic approximations or empirical data are often used, inevitably introducing uncertainties. Additionally, uncertainties may stem from inaccurate measurements of initial or boundary conditions, as well as from source terms, further compounding the uncertainties in the model. For numerical studies of the Boltzmann equation and other kinetic models with or without randomness, we refer readers to works such as [28, 36, 38, 51] and [19, 29, 30, 48, 49], and particularly for the linear Boltzmann equation [40, 52]. Among the various numerical approaches, the generalized polynomial chaos (gPC)-based stochastic Galerkin (SG) method and its variations have been widely adopted, demonstrating success in a range of applications [62]. Beyond numerical simulations, theoretical studies have established the stability and convergence of these methods. Spectral convergence for the gPC-based SG method was demonstrated in [27, 43, 44], while [42] and [18] introduced a robust framework based on hypocoercivity to perform local sensitivity analysis for a class of multiscale, inhomogeneous kinetic equations with random uncertainties—approximated using the gPC-based SG method. For further reference, we point readers to the recent collection [37] and the survey [50].

An important approximation strategy in kinetic theory is given by Grad's moment method [22, 23] based on the expansion of the distribution function in Hermite polynomials, which extends the set of variables of a continuum model beyond the fields of density, velocity, and temperature. The additional variables are given by higher-order moments of the distribution function. Indeed, to describe the kinetic effects in highly non-equilibrium regimes, many moments are needed which results in a large systems of PDEs to be solved. It is known that Struchtrup and Torrilhon [58] have rigorously derived the regularized 13-moment equations from the Boltzmann equation of the monatomic gases. The final system consists of evolution equations for the 13 fields of density, velocity, temperature, stress tensor and heat flux. See [39] for regularized moment equations and moment closure hierarchies for kinetic theory. In 1950's, Grad solved the closure problem by assuming the distribution can be expressed around the Maxwellian function. According to [57], Grad's choice, or other nonlinear closure such as Pearson's [59] is problematic, as it exhibits negative values in the tail for non-vanishing heat flux, which could be the reason for the loss of hyperbolicity of the moment equations. In general, the moment closure is a challenging and important problem in the approximation theory for kinetic models. Many numerical computational methods have been developed based on the Grad moment approach [11, 12]. However, these closure conditions may not be valid in practice, especially when there are shock profiles or complicated boundary conditions. We list some works here: for examples the P_N model [14], the filtered P_N model [53], the positive P_N model [26], the entropy-based M_N model [2] and the MP_N model [20, 21, 41]. In this work, our goal is to use the machine learning approach to find an accurate closure system.

With the recent development of data-driven methodology and machine learning (ML) techniques, some new approaches based on machine learning and neural networks have been proposed to solve the moment closure problem; since the relationship between the highest-order moment and lower-order moments is generally unknown, aside from the assumption that such a relationship exists, a neural network appears to be an ideal candidate to serve as a black-box model representing this relationship after training from the data, which are obtained by solving the kinetic equation. One of the groundbreaking frameworks is in [25] by Han *et al.*, where they first used an autoencoder to learn a set of generalized moments that optimally represent the underlying velocity distribution, and then trained a moment closure model for these generalized moments to effectively capture the dynamics associated with the kinetic equation. By utilizing the conservation-dissipation formalism, a stable closure model is developed from irreversible thermodynamics for the Boltzmann-BGK equation in [34], parameterized by a multilayer perceptron. In addition, Bois *et al.* in [5] introduced a nonlocal closure model for the Vlasov-Poisson system using a convolutional neural network. Furthermore, in [45, 61], the widely recognized Hammett-Perkins Landau fluid closure model was studied by ML and neural network techniques. In particular, we highlight the recent work [31] by

Huang *et al.*, where they develop a new ML framework for the moment closure problem of the radiative transfer equation (RTE).

For the moment closure problems, the hyperbolicity of the derived moment system is critical to the well-posedness of the first-order partial differential equations [55]. In fact, Grad’s pioneering work on moment closure in gas kinetic theory, presented in [22], laid the foundation for moment models. However, it was later shown in [10] that in the three-dimensional case, the equilibrium state for Grad’s 13-moment model lies on the boundary of the hyperbolicity region. This limitation significantly restricts the applicability of the moment method. Consequently, this issue has garnered considerable attention, with numerous studies in the literature [8, 9, 20] dedicated to developing globally hyperbolic moment systems. The classical philosophy in deriving and solving the moment system, instead of the kinetic equations themselves, is to pursue the balance between generic accuracy and practical computability. However, with recent advancements in ML and data-driven modeling [6, 24], novel ML-based approaches [5, 25, 45, 47, 54] have emerged to address the moment closure problem, offering new potential for both accuracy and practicality. We refer the readers to [31] and the references therein for more recent progress in this field. Albeit the success of ML in the application of moment closure problems, it is worth mentioning that most of the aforementioned works do not ensure hyperbolicity or long-term stability, with the exception of the work in [34], where a stable ML-based closure model is proposed with hyperbolicity and Galilean invariance for the BGK equation, a simplified Boltzmann kinetic equation, though this model is restricted to a single additional nonequilibrium variable.

Motivation and our contributions: In this paper, we focus on developing an ML-based moment closure model for the linearized Boltzmann equation in semiconductor devices, addressing both deterministic and stochastic cases. Classical moment closure approaches approximate unclosed higher-order moments based on empirical assumptions, which may not hold in general [10]. Additionally, unclosed higher-order moments often vary widely in magnitude and can become very small on certain scales, such as in the optically thick regime for RTE [31]. This variability complicates neural network training, as the target function may be difficult to learn directly from lower-order moments without appropriate output normalization [5]. Therefore, rather than directly learning the unclosed higher-order moments [25], we opt to learn the spatial gradient of the unclosed moment using neural networks, drawing on a similar strategy proposed for RTE [31]. For the deterministic case, we first derive the unclosed moment system using Hermite polynomials and their recurrence relations. A neural network incorporating gradients of lower-order moments with natural output normalization is then introduced to learn the gradient of the highest-order moment. To ensure long-term stability, we also introduce an approach inspired by [17, 32, 33] that enforces global hyperbolicity in the ML-based moment closure model. This is achieved by constructing a symmetrizer (i.e., a symmetric positive definite matrix) for the closure system and deriving constraints that make the system globally symmetrizable hyperbolic.

For the stochastic case, we use the gPC-based SG method to discretize the random variable and derive a higher-dimensional deterministic moment system. The gradient-learning approach is also applied to this system, enabling an ML-based moment closure model.

Organization of our paper: The rest of this paper is organized as follows: We first introduce the semi-conductor Boltzmann equation and its associated moment closure problem in Section 2. In Section 3, we propose an ML-based moment closure model to learn the unclosed highest-order moment, where the random variables are handled by the stochastic Galerkin method. The training process of the neural networks including the data generation is presented in Section 4. We validate our proposed ML-based moment closure model by numerical examples in Section 5. Some conclusion remarks are given in Section 6.

2 Semiconductor Boltzmann equation and moments system

2.1 Semiconductor Boltzmann equation

The linear Boltzmann equation for semiconductor devices with random parameters is given by

$$\partial_t f(t, x, v, z) + v \partial_x f(t, x, v, z) = Q(f)(t, x, v, z), \quad (1)$$

with the initial condition

$$f(0, x, v, z) = f^0(x, v, z), \quad (2)$$

where $f = f(t, x, v, z)$ is the probability density function at time t and position $x \in \mathbb{R}$, with velocity variable $v \in \mathbb{R}$ and random variable $z \in I_z \subset \mathbb{R}^{d_z}$ characterizes the random inputs. Here, the collision operator $Q(f)$ describes a linear approximation of the electron-photon interaction, given by

$$Q(f)(v, z) = \int_{\mathbb{R}} \sigma(v, v_*, z) [M(v) f(v_*, z) - M(v_*) f(v, z)] dv_*, \quad (3)$$

where $M(v)$ is the normalized Maxwellian distribution

$$M(v) := \frac{1}{(2\pi)^{1/2}} e^{-|v|^2}. \quad (4)$$

In this paper, In this paper, we consider the one-dimensional in space and velocity variables, with uncertain parameters arising from:

- (i) the initial datum $f^0(x, v, z)$;
- (ii) the collision kernel $\sigma(v, v_*, z) \geq 0$.

In particular, if we assume the scattering kernel to be isotropic (independent of the velocity variable), i.e., $\sigma(v, v_*, z) = \sigma(z)$, the equation becomes

$$\begin{aligned} & \partial_t f(t, x, v, z) + v \partial_x f(t, x, v, z) \\ &= \sigma(z) M(v) \left(\int_{\mathbb{R}} f(t, x, v_*, z) dv_* \right) - \sigma(z) f(t, x, v, z). \end{aligned} \quad (5)$$

2.2 Moments system

We take the moments of the linearized Boltzmann equation against the Hermite polynomials of v in the whole space, instead of the bounded domain as for RTE [31]. Denoting the k -th order Hermite polynomial by $H_k = H_k(v)$ for $k \geq 0$, the k -th order moments can be defined as

$$m_k(t, x, z) := \int_{\mathbb{R}} f(t, x, v, z) H_k(v) dv, \quad k \geq 0. \quad (6)$$

Remark 1 Recall the recurrence relation of the Hermite polynomials:

$$H_{k+1}(v) = \sqrt{\frac{2}{k+1}} v H_k(v) - \sqrt{\frac{k}{k+1}} H_{k-1}(v) \quad (7)$$

with $H_0(v) = \pi^{-\frac{1}{4}}$ and $H_1(v) = \sqrt{2}\pi^{-\frac{1}{4}}v$. Furthermore, the orthogonal relation with respect to the weight function $M(v)$ holds:

$$\int_{\mathbb{R}} H_m(v) H_n(v) M(v) dv = 0, \quad \text{for all } m \neq n. \quad (8)$$

Hence, multiplying both sides of (5) by $H_k(v)$ and integrating over the whole velocity space \mathbb{R} lead to

$$\begin{aligned} & \partial_t \int_{\mathbb{R}} H_k(v) f(t, x, v, z) dv + \partial_x \int_{\mathbb{R}} v H_k(v) f(t, x, v, z) dv \\ &= \sigma(z) \pi^{\frac{1}{4}} \int_{\mathbb{R}} H_0(v) H_k(v) M(v) dv \left(\int_{\mathbb{R}} f(t, x, v_*, z) dv_* \right) \\ & \quad - \sigma(z) \int_{\mathbb{R}} H_k(v) f(t, x, v, z) dv, \end{aligned} \quad (9)$$

which, by considering the definition of (6), involving the recurrence relation (7) on the left-hand side and the orthogonal relation (8) on the right-hand side of (9) above, can be further simplified as

$$\begin{aligned} \partial_t m_k(t, x, z) + \partial_x \left[\sqrt{\frac{k+1}{2}} m_{k+1}(t, x, z) + \sqrt{\frac{k}{2}} m_{k-1}(t, x, z) \right] \\ = \delta_{0k} \sigma(z) m_0(t, x, z) - \sigma(z) m_k(t, x, z). \end{aligned} \quad (10)$$

Therefore, the moment system up to m_N is presented as follows:

$$\left\{ \begin{array}{l} \partial_t m_0 + \sqrt{\frac{1}{2}} \partial_x m_1 = 0, \\ \partial_t m_1 + \partial_x m_2 + \sqrt{\frac{1}{2}} \partial_x m_0 = -\sigma(z) m_1, \\ \partial_t m_2 + \sqrt{\frac{3}{2}} \partial_x m_3 + \partial_x m_1 = -\sigma(z) m_2, \\ \dots \\ \dots \\ \dots \\ \partial_t m_N + \sqrt{\frac{N+1}{2}} \partial_x m_{N+1} + \sqrt{\frac{N}{2}} \partial_x m_{N-1} = -\sigma(z) m_N. \end{array} \right. \quad (11)$$

We can find that, in the last equation of (11) above, the evolution of N -th order moment m_N depends on m_{N+1} , therefore, the moments system (11) is unclosed. In fact, there are many classical ways to close the system, where the P_N model [14] is the most straightforward approach. The P_N model utilizes the orthogonal polynomials in the velocity space and assumes $m_{N+1} = 0$ to close the model, such that the system (11) can be written in the following vector form: by denoting $\mathbf{m} = (m_0, m_1, \dots, m_N)^T$,

$$\partial_t \mathbf{m} + A \partial_x \mathbf{m} = S \mathbf{m}, \quad (12)$$

where the diagonal coefficient matrix $S \in \mathbb{R}^{(N+1) \times (N+1)}$ is

$$S := \text{diag}(0, -\sigma(z), -\sigma(z), \dots, -\sigma(z)), \quad (13)$$

and the coefficient matrix $A \in \mathbb{R}^{(N+1) \times (N+1)}$ is

$$A := \begin{pmatrix} 0 & \sqrt{\frac{1}{2}} & 0 & 0 & 0 & 0 & \dots & 0 \\ \sqrt{\frac{1}{2}} & 0 & 1 & 0 & 0 & 0 & \dots & 0 \\ 0 & 1 & 0 & \sqrt{\frac{3}{2}} & 0 & 0 & \dots & 0 \\ \vdots & \vdots & \vdots & \vdots & \ddots & \ddots & \ddots & \vdots \\ \vdots & \vdots & \vdots & \vdots & \ddots & \ddots & \ddots & \vdots \\ 0 & 0 & \dots & 0 & \sqrt{\frac{N-2}{2}} & 0 & \sqrt{\frac{N-1}{2}} & 0 \\ 0 & 0 & \dots & 0 & 0 & \sqrt{\frac{N-1}{2}} & 0 & \sqrt{\frac{N}{2}} \\ 0 & 0 & \dots & 0 & 0 & 0 & \sqrt{\frac{N}{2}} & 0 \end{pmatrix}. \quad (14)$$

3 Machine learning based moments closure model

Recent advancements in ML techniques have led to notable progress in using ML frameworks to enhance moment closure models. One of the standard ways for the moments closure is to seek the relation between the highest moment m_{N+1} and the lower-order moments [25]:

$$m_{N+1} = \mathcal{N}(m_0, m_1, \dots, m_N),$$

where $\mathcal{N} : \mathbb{R}^{N+1} \mapsto \mathbb{R}$ is a neural network trained from data. This is the so-called Learning the Moment (LM) approach. In [25], it served as the regression in supervised learning and a part of the end-to-end learning procedure.

3.1 Formulation and hyperbolic condition

In order to close the moment system (11) and circumvent the challenge in the LM framework, where the training process often converges to a local minimum, we will adopt the closure relation introduced in [31]. This approach assumes a linear relationship between the gradient of the highest moment, $\partial_x m_{N+1}$, and the gradients of lower-order moments, $\partial_x m_0, \dots, \partial_x m_N$, as follows:

$$\partial_x m_{N+1} = \sum_{i=0}^N \mathcal{N}_i(m_0, m_1, \dots, m_N) \partial_x m_i. \quad (15)$$

In this case, we can rewrite the moments system (11) in the following vector form:

$$\partial_t \mathbf{m} + A \partial_x \mathbf{m} = S \mathbf{m}, \quad (16)$$

where the diagonal coefficient matrix $S \in \mathbb{R}^{(N+1) \times (N+1)}$ is

$$S := \text{diag}(0, -\sigma(z), -\sigma(z), \dots, -\sigma(z)), \quad (17)$$

and the coefficient matrix $A \in \mathbb{R}^{(N+1) \times (N+1)}$ is

$$A := \begin{pmatrix} 0 & \sqrt{\frac{1}{2}} & 0 & 0 & 0 & 0 & \cdots & 0 \\ \sqrt{\frac{1}{2}} & 0 & 1 & 0 & 0 & 0 & \cdots & 0 \\ 0 & 1 & 0 & \sqrt{\frac{3}{2}} & 0 & 0 & \cdots & 0 \\ \vdots & \vdots & \vdots & \vdots & \ddots & \ddots & \ddots & \vdots \\ \vdots & \vdots & \vdots & \vdots & \ddots & \ddots & \ddots & \vdots \\ 0 & 0 & \cdots & 0 & \sqrt{\frac{N-2}{2}} & 0 & \sqrt{\frac{N-1}{2}} & 0 \\ 0 & 0 & \cdots & 0 & 0 & \sqrt{\frac{N-1}{2}} & 0 & \sqrt{\frac{N}{2}} \\ a_0 & a_1 & \cdots & a_{N-4} & a_{N-3} & a_{N-2} & a_{N-1} & a_N \end{pmatrix} \quad (18)$$

with coefficients a_i in the last row of A and \mathcal{N}_i satisfying the following relation:

$$a_j = \begin{cases} \sqrt{\frac{N+1}{2}} \mathcal{N}_j, & j \neq N-1, \\ \sqrt{\frac{N+1}{2}} \mathcal{N}_j + \sqrt{\frac{N}{2}}, & j = N-1. \end{cases} \quad (19)$$

In general, the matrix A is not real-diagonalizable, so the system is not necessarily hyperbolic. We are trying to find a condition that enforces A to be hyperbolic, so that the system (16) remains stable over time. To achieve this, we follow the technique introduced in [33], i.e., we seek an SPD matrix A_0 such that $A_0 A$ is symmetric. However, this matrix A_0 is usually hard to compute. Therefore, without loss of generality, we relax the assumption (15) by removing the first k dependence that

$$\partial_x m_{N+1} = \sum_{i=N-k}^N \mathcal{N}_i(m_0, m_1, \dots, m_N) \partial_x m_i,$$

where $k = 2, 3$ are typical choices to simplify the computation, and in either case, we assume $N \geq 3$ to avoid the trivial results. In what follows, we will take $k = 2$ to illustrate the idea, whereas the same strategy can be extended directly to $k = 3$.

Theorem 1 Consider the matrix $A \in \mathbb{R}^{(N+1) \times (N+1)}$ with $N \geq 3$ and $k = 2$ in (18), i.e.,

$$A = \begin{pmatrix} 0 & \sqrt{\frac{1}{2}} & 0 & 0 & 0 & 0 & \cdots & 0 \\ \sqrt{\frac{1}{2}} & 0 & 1 & 0 & 0 & 0 & \cdots & 0 \\ 0 & 1 & 0 & \sqrt{\frac{3}{2}} & 0 & 0 & \cdots & 0 \\ \vdots & \vdots & \vdots & \vdots & \ddots & \ddots & \ddots & \vdots \\ \vdots & \vdots & \vdots & \vdots & \ddots & \ddots & \ddots & \vdots \\ 0 & 0 & \cdots & 0 & \sqrt{\frac{N-2}{2}} & 0 & \sqrt{\frac{N-1}{2}} & 0 \\ 0 & 0 & \cdots & 0 & 0 & \sqrt{\frac{N-1}{2}} & 0 & \sqrt{\frac{N}{2}} \\ 0 & 0 & \cdots & 0 & 0 & a_{N-2} & a_{N-1} & a_N \end{pmatrix}$$

where a_j is defined as in (19). If the constraints of the coefficients $a_j, j = N-2, N-1, N$ hold:

$$\sqrt{\frac{N-1}{2}} a_{N-1} + a_N a_{N-2} - \sqrt{\frac{N}{2}} a_{N-2}^2 > 0, \quad (20)$$

or equivalently, for $\mathcal{N}_j, j = N-2, N-1, N$,

$$\frac{N+1}{2} \left(\mathcal{N}_{N-2} \mathcal{N}_N - \sqrt{\frac{N}{2}} \mathcal{N}_{N-2}^2 \right) + \sqrt{\frac{N-1}{2}} \left(\sqrt{\frac{N+1}{2}} \mathcal{N}_{N-1} + \sqrt{\frac{N}{2}} \right) > 0, \quad (21)$$

then there exists an SPD matrix $A_0 = \begin{pmatrix} I & 0 \\ 0 & B \end{pmatrix}$ such that A_0A is symmetric, where $I \in \mathbb{R}^{(N-1) \times (N-1)}$ is an identity matrix, and $B = \begin{pmatrix} b_1 & b_2 \\ b_2 & b_3 \end{pmatrix}$ is an SPD matrix.

Proof Since A_0A is required to be a real symmetric matrix, we perform the matrix multiplication and impose the condition that the corresponding entries be equal, thereby ensuring that A_0A is symmetric. This leads to the following equations:

$$\begin{cases} \sqrt{\frac{N-1}{2}}b_1 + a_{N-2}b_2 = \sqrt{\frac{N-1}{2}}, \\ \sqrt{\frac{N-1}{2}}b_2 + a_{N-2}b_3 = 0, \\ \sqrt{\frac{N}{2}}b_1 + a_Nb_2 = a_{N-1}b_3, \end{cases} \quad (22)$$

which can be further written in matrix form $\mathbf{M}\mathbf{b} = \mathbf{c}$ with

$$\mathbf{M} = \begin{pmatrix} \sqrt{\frac{N-1}{2}} & a_{N-2} & 0 \\ 0 & \sqrt{\frac{N-1}{2}} & a_{N-2} \\ \sqrt{\frac{N}{2}} & a_N & -a_{N-1} \end{pmatrix}, \quad \mathbf{b} = \begin{pmatrix} b_1 \\ b_2 \\ b_3 \end{pmatrix}, \quad \mathbf{c} = \begin{pmatrix} \sqrt{\frac{N-1}{2}} \\ 0 \\ 0 \end{pmatrix}.$$

Then, using the Cramer's rule to solve (22) above, we find

$$\begin{cases} b_1 = \frac{\sqrt{\frac{N-1}{2}}(-\sqrt{\frac{N-1}{2}}a_{N-1} - a_Na_{N-2})}{\sqrt{\frac{N-1}{2}}(-\sqrt{\frac{N-1}{2}}a_{N-1} - a_Na_{N-2}) + \sqrt{\frac{N}{2}}a_{N-2}^2}, \\ b_2 = \frac{\sqrt{\frac{N-1}{2}}\sqrt{\frac{N}{2}}a_{N-2}}{\sqrt{\frac{N-1}{2}}(-\sqrt{\frac{N-1}{2}}a_{N-1} - a_Na_{N-2}) + \sqrt{\frac{N}{2}}a_{N-2}^2}, \\ b_3 = \frac{-\sqrt{\frac{N}{2}}\sqrt{\frac{N-1}{2}}}{\sqrt{\frac{N-1}{2}}(-\sqrt{\frac{N-1}{2}}a_{N-1} - a_Na_{N-2}) + \sqrt{\frac{N}{2}}a_{N-2}^2}. \end{cases} \quad (23)$$

Considering the fact that B is an SPD matrix, by Sylvester's criterion, it has to satisfy the following inequalities:

$$\begin{cases} b_1 > 0, \\ b_1b_3 - b_2^2 > 0, \end{cases} \quad (24)$$

from which, it is clear that $b_3 > 0$, i.e.,

$$\sqrt{\frac{N-1}{2}} \left(-\sqrt{\frac{N-1}{2}}a_{N-1} - a_Na_{N-2} \right) + \sqrt{\frac{N}{2}}a_{N-2}^2 < 0.$$

Since $b_1 > 0$, we must have $\sqrt{\frac{N-1}{2}}a_{N-1} + a_N a_{N-2} > 0$. On the other hand, to achieve $b_1 b_3 - b_2^2 > 0$, we have $\sqrt{\frac{N-1}{2}}a_{N-1} + a_N a_{N-2} - \sqrt{\frac{N}{2}}a_{N-2}^2 > 0$. Hence, considering $N \geq 3$, all these inequalities can be summarized into a single constraint (20).

Finally, by substituting (19) into (20), we can obtain the constraint (21) that should be satisfied by \mathcal{N}_j , $j = N-2, N-1, N$.

Remark 2 If $N = 1$, we have no other option but to set $k = 1$. In this case, the hyperbolic constraint is given by $a_0 > 0$, or equivalently, $\mathcal{N}_0 > -\sqrt{\frac{N}{N+1}}$.

3.2 Stochastic Galerkin (SG) method for random variable

In this subsection, we discuss how to manage the random variable z existing in the moment system (11). The main idea involves applying the stochastic Galerkin (SG) method to eliminate the randomness, thereby transforming the system into an equivalent form containing only deterministic coefficients. For simplicity of notation, we assume $z \in I_z \subset \mathbb{R}^{d_z}$ with $d_z = 1$ throughout the rest of this paper, which can be generalized to high dimension without an essential difference.

We define the space

$$\mathbb{P}^K := \text{Span} \left\{ \phi_i(z) \mid 0 \leq i \leq K \right\}$$

equipped with the inner product with respect to the probability density function $\pi(z)$ in z :

$$\langle f(t, x, v, \cdot), g(t, x, v, \cdot) \rangle_{I_z} = \int_{I_z} f(t, x, v, z) \overline{g(t, x, v, z)} \pi(z) dz,$$

where $\{\phi_i(z)\}_{i=0}^K$ is an orthonormal gPC basis function, i.e.,

$$\int_{I_z} \phi_i(z) \phi_j(z) \pi(z) dz = \delta_{ij}, \quad 0 \leq i, j \leq K. \quad (25)$$

Then, the typical SG method is based on seeking an approximation of $f(z)$ in \mathbb{P}^K such that

$$f(z) \approx \sum_{i=0}^K f^i \phi_i(z) \quad \text{with} \quad f^i = \int_{I_z} f(z) \phi_i(z) \pi(z) dz. \quad (26)$$

Now, in the case of (11), we can expand $m_k(t, x, z)$ as follows:

$$m_k(t, x, z) \approx \sum_{i=0}^K m_k^i(t, x) \phi_i(z) \quad (27)$$

with

$$m_k^i(t, x) = \int_{I_z} m_k(t, x, z) \phi_i(z) \pi(z) dz. \quad (28)$$

More precisely, considering the k -th equation in (11),

$$\begin{aligned} \partial_t m_k(t, x, z) + \sqrt{\frac{k+1}{2}} \partial_x m_{k+1}(t, x, z) + \sqrt{\frac{k}{2}} \partial_x m_{k-1}(t, x, z) \\ = -\sigma(z) m_k(t, x, z), \end{aligned} \quad (29)$$

and following (27), we can project both sides of (29) into \mathbb{P}^K and obtain

$$\begin{aligned} \partial_t m_k^i(t, x) + \sqrt{\frac{k+1}{2}} \partial_x m_{k+1}^i(t, x) + \sqrt{\frac{k}{2}} \partial_x m_{k-1}^i(t, x) \\ = \sum_{j=0}^K S_{ij} m_k^j(t, x), \end{aligned} \quad (30)$$

for $k \geq 1$ and $0 \leq i \leq K$, where the matrix $S = (S_{ij}) \in \mathbb{R}^{(K+1) \times (K+1)}$ includes pre-computed weights concerning the random collision kernel $\sigma(z)$ as follows:

$$S_{ij} = \int_{I_z} -\sigma(z) \phi_j(z) \phi_i(z) \pi(z) dz.$$

Furthermore, by denoting $\mathbf{m}_k(t, x) = (m_k^0(t, x), m_k^1(t, x), \dots, m_k^K(t, x))^T$, we can rewrite (30) in the following vector form,

$$\partial_t \mathbf{m}_k + \sqrt{\frac{k+1}{2}} \partial_x \mathbf{m}_{k+1} + \sqrt{\frac{k}{2}} \partial_x \mathbf{m}_{k-1} = \mathbf{S} \mathbf{m}_k, \quad (31)$$

for $k \geq 1$, and

$$\partial_t \mathbf{m}_0 + \sqrt{\frac{1}{2}} \partial_x \mathbf{m}_1 = \mathbf{0},$$

for $k = 0$.

Again, we need to propose a closure relation before we can solve the system. We follow the same dependence as in (15) and assume:

$$\partial_x \mathbf{m}_{N+1} = \sum_{i=0}^N \mathcal{N}_i(\mathbf{m}_0, \mathbf{m}_1, \dots, \mathbf{m}_N) \partial_x \mathbf{m}_i. \quad (32)$$

Then, by inserting (32) into (31) and denoting $\mathbf{m} = (\mathbf{m}_0, \mathbf{m}_1, \dots, \mathbf{m}_N)^T$, the moment system via SG method can be written as:

$$\partial_t \mathbf{m} + \mathbf{A} \partial_x \mathbf{m} = \mathbf{S} \mathbf{m}, \quad (33)$$

where

$$\mathbf{A} = \begin{pmatrix} 0 & \sqrt{\frac{1}{2}}\mathbf{I}_{K+1} & 0 & 0 & 0 & 0 & \cdots & 0 \\ \sqrt{\frac{1}{2}}\mathbf{I}_{K+1} & 0 & \mathbf{I}_{K+1} & 0 & 0 & 0 & \cdots & 0 \\ 0 & \mathbf{I}_{K+1} & 0 & \sqrt{\frac{3}{2}}\mathbf{I}_{K+1} & 0 & 0 & \cdots & 0 \\ \vdots & \vdots & \vdots & \vdots & \ddots & \ddots & \ddots & \vdots \\ \vdots & \vdots & \vdots & \vdots & \ddots & \ddots & \ddots & \vdots \\ 0 & 0 & \cdots & 0 & \sqrt{\frac{N-2}{2}}\mathbf{I}_{K+1} & 0 & \sqrt{\frac{N-1}{2}}\mathbf{I}_{K+1} & 0 \\ 0 & 0 & \cdots & 0 & 0 & \sqrt{\frac{N-1}{2}}\mathbf{I}_{K+1} & 0 & \sqrt{\frac{N}{2}}\mathbf{I}_{K+1} \\ \mathbf{a}_0 & \mathbf{a}_1 & \cdots & \mathbf{a}_{N-4} & \mathbf{a}_{N-3} & \mathbf{a}_{N-2} & \mathbf{a}_{N-1} & \mathbf{a}_N \end{pmatrix}$$

with

$$\mathbf{a}_j = \begin{cases} \sqrt{\frac{N+1}{2}}\mathcal{N}_j, & j \neq N-1, \\ \sqrt{\frac{N+1}{2}}\mathcal{N}_j + \sqrt{\frac{N}{2}}, & j = N-1. \end{cases}$$

and

$$\mathbf{S} = \text{diag}(0, S, S, \dots, S).$$

In fact, when applying the SG method, we are often interested in the moments' expectation $\mathbb{E}(m_k)$ and standard deviation $s(m_k)$, which are closely related to the coefficients in (27). Without loss of generality, we assume $\phi_0(z) = 1$ such that for each moment m_k , we have,

$$\begin{aligned} \mathbb{E}(m_k) &\approx \mathbb{E}\left(\sum_{i=0}^K m_k^i \phi_i\right) \\ &= \int_{I_z} \sum_{i=0}^K m_k^i(t, x) \phi_i(z) \pi(z) dz \\ &= \sum_{i=0}^K m_k^i(t, x) \int_{I_z} \phi_0(z) \phi_i(z) \pi(z) dz = m_k^0(t, x), \end{aligned} \quad (34)$$

where we apply the orthonormality of $\{\phi_i(z)\}$ in the last equality above.

For the standard deviation, we have,

$$s(m_k) \approx \sqrt{\mathbb{E}\left(\sum_{i=0}^K m_k^i \phi_i\right)^2 - (m_k^0)^2} = \sqrt{\sum_{i=1}^K (m_k^i)^2}. \quad (35)$$

4 Training and methodology

In this section, we present the details about learning $\partial_x m_{N+1}$ by the lower orders of moments, and using the WENO scheme to solve the system after $\partial_x m_{N+1}$ is properly approximated. We will deal with both the deterministic case and the corresponding UQ problem. Numerical results of both cases will be presented in the next Section 5.

4.1 Data preparation

One key ingredient of our methodology is to approximate the highest moment using the lower orders of moments. To achieve this goal, we need to train a neural network $\mathcal{N} = (\mathcal{N}_0, \dots, \mathcal{N}_N) : \mathbb{R}^{N+1} \rightarrow \mathbb{R}^{N+1}$ as in (15) for the deterministic problem or a network $\mathcal{N} = (\mathcal{N}_0, \dots, \mathcal{N}_N) : \mathbb{R}^{(K+1) \times (N+1)} \rightarrow \mathbb{R}^{(K+1) \times (N+1)}$ as in (32) for the stochastic case. The first step of our training process is to prepare training data to fit in our models. We will use synthetic data, ie: reference solutions for the moments obtained from classical numerical algorithms, to serve as the input and labels of our networks.

In the case of the deterministic model (15)-(16), we apply the method given by Jin and Pareschi in [37] to solve the deterministic counterpart of (1) (no z) and obtain the reference solution $f(t, x, v)$. For simplicity, we consider the one dimension in space x and velocity v for illustration, where we set the computational domain of x to be $[0, 1]$ with grid points $N_x = 100$, and apply $N_v = 8$ for velocity discretization. Following the CFL condition, the time step size is chosen as $\Delta t = 0.1\Delta x$ with the final time $t = 0.5$. Once $f(t, x, v)$ is obtained, we compute the k -th moment $m_k(t, x)$ by integrating f against the corresponding Hermite polynomial H_k , as introduced in (6), where the Gauss-Hermite quadrature rule with $N_v = 8$ is used for integral evaluation.

In the case of the moment system with uncertainty (32)-(33), we need to compute reference solutions $m_k^i(t, x)$, which is the i -th Galerkin coefficient of the k -th moment as defined in (27). Based on the stochastic collocation (SC) method [62], we can obtain the coefficients $m_k^i(t, x)$ as in (28). To this end, the integral in (28) is evaluated by

$$\int_{I_z} m_k(t, x, z) \phi_i(z) \pi(z) dz \approx \sum_{j=1}^M m_k(t, x, z_j) \phi_i(z_j) \pi(z_j) w_j, \quad (36)$$

where (z_j, w_j) are the collocation points and corresponding weights with M -quadrature nodes, and $m_k(t, x, z_j)$ are obtained similarly as in the deterministic case at each z_j .

4.2 Training

In this subsection, we discuss the details of the architecture and the training process of the neural networks (\mathcal{N} or \mathcal{N}) mentioned in the subsection above.

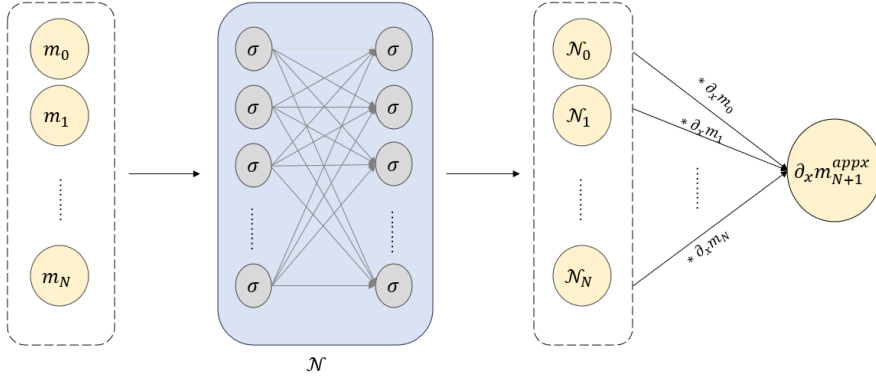


Fig. 1 Architecture of our neural network.

The architecture (Figure 1) we choose is a standard fully connected neural network, where the input consists of lower moments (or their Galerkin coefficients in the UQ setting). This network is designed with 5 hidden layers, each containing 256 nodes, and employs the ReLU activation function. The output dimension matches that of the input. Figure 1 provides a graphical representation of this architecture. If hyperbolic condition is considered, we follow the same construction in [33] to modify the output layer to incorporate hyperbolicity into our model.

To train the neural networks, we apply the Adam optimizer with the learning rate 10^{-3} initially. The total number of training epochs is 1000 and the learning rate is set to decrease to 0.35 every 100 epochs. We let the batch size be 1024. The input is normalized with zero mean and unit variance. These training hyperparameters are used in both deterministic and stochastic tests, and the only difference between the networks \mathcal{N} and \mathcal{N} is the size of the input and output. We use 90% of the data to train the networks and the rest of the data for validation. The hyperparameters and the activation function are tuned to minimize the loss function, which we describe below.

In the last subsection above, we have discussed how to obtain the reference solution for $m_k, \partial_x m_k$ in the deterministic problem and $m_k^i, \partial_x m_k^i$ in the stochastic problem, for which we denote “true” in the superscript as follows:

$$\begin{aligned}
 \mathbf{m}_{det}^{true} &= (m_0^{true}, \dots, m_N^{true}), \\
 \mathbf{m}_{sto}^{true} &= (\mathbf{m}_0^{true}, \dots, \mathbf{m}_N^{true}) \text{ with } \mathbf{m}_k^{true} = (m_k^{0,true}, \dots, m_k^{K,true}), \\
 \partial_x \mathbf{m}_{det}^{true} &= (\partial_x m_0^{true}, \dots, \partial_x m_N^{true}), \\
 \partial_x \mathbf{m}_{sto}^{true} &= (\partial_x \mathbf{m}_0^{true}, \dots, \partial_x \mathbf{m}_N^{true}) \text{ with } \partial_x \mathbf{m}_k^{true} = (\partial_x m_k^{0,true}, \dots, \partial_x m_k^{K,true}).
 \end{aligned} \tag{37}$$

Then, in the architecture shown in Figure 1, the $\partial_x m_{N+1}^{appx}$ stand for the approximation from the neural network \mathcal{N} in the deterministic case: following

(15),

$$\partial_x m_{N+1}^{appx}(x_j, t_n) = \langle \mathcal{N}(\mathbf{m}_{det}^{true}(x_j, t_n)), \partial_x \mathbf{m}_{det}^{true}(x_j, t_n) \rangle, \quad (38)$$

where $\langle \cdot \rangle$ is the inner product in the standard Euclidean space. The approximation in the stochastic case is denoted by $\partial_x \mathbf{m}_{N+1}^{appx}(x_j, t_n)$ in a similar manner.

Now, we are in a position to introduce the loss functions for our neural networks in both the deterministic and the stochastic settings:

$$\mathcal{L}_{det} := \frac{1}{N_{data}} \sum_{j,n} |\partial_x m_{N+1}^{true}(x_j, t_n) - \partial_x m_{N+1}^{appx}(x_j, t_n)|^2, \quad (39)$$

$$\mathcal{L}_{sto} := \frac{1}{N_{data}} \sum_{j,n} \|\partial_x \mathbf{m}_{N+1}^{true}(x_j, t_n) - \partial_x \mathbf{m}_{N+1}^{appx}(x_j, t_n)\|_2^2, \quad (40)$$

and we will measure the accuracy of our moment closure models by evaluating the relative L^2 errors between the approximated solutions by neural networks and reference solutions by solving the kinetic equation as follows:

$$E_{2,det} := \sqrt{\frac{\sum_{j,n} |\partial_x m_{N+1}^{true}(x_j, t_n) - \partial_x m_{N+1}^{appx}(x_j, t_n)|^2}{\sum_{j,n} |\partial_x m_{N+1}^{true}(x_j, t_n)|^2}}, \quad (41)$$

$$E_{2,sto} = \sqrt{\frac{\sum_{j,n} \|\partial_x \mathbf{m}_{N+1}^{true}(x_j, t_n) - \partial_x \mathbf{m}_{N+1}^{appx}(x_j, t_n)\|_2^2}{\sum_{j,n} \|\partial_x \mathbf{m}_{N+1}^{true}(x_j, t_n)\|_2^2}}. \quad (42)$$

In Figure 2, we present the relative L^2 errors with respect to epochs by using our architecture to train $\partial_x m_{N+1}$ in the deterministic problem. We compare the performances when $N = 1, 3, 5$ with $\sigma = 2$ and $\sigma = 10$. We observe that when $\sigma = 2$, the error is significant if the number of moments we choose to close the system is small (say $N = 1$). In both cases, the saturated error becomes smaller as N increases.

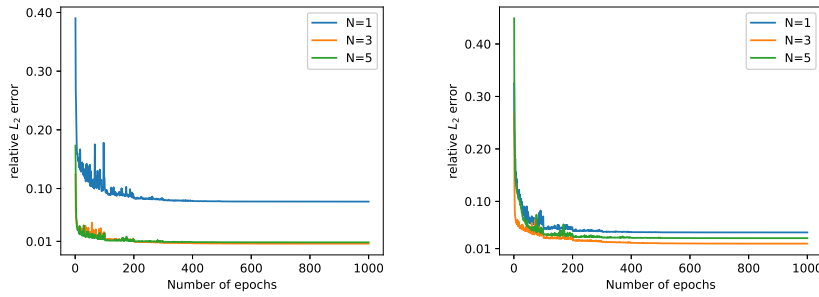


Fig. 2 Left: Relative L^2 errors of (41) for different N with $\sigma = 2$. Right: Relative L^2 errors of (41) for different N with $\sigma = 10$.

4.3 WENO Scheme

Once $\partial_x m_{N+1}$ is properly learned using the lower-order moments, we need to solve the systems (16) and (33) using some classical numerical schemes. The scheme we choose is the fifth-order finite difference WENO scheme with a Lax-Friedrichs flux-splitting for spatial discretization [35]. We take the grid number in space to be $N_x = 100$. For the time discretization, we apply the third-order strong-stability-preserving Runge-Kutta (RK) scheme [56] with CFL condition $\Delta t = 0.1\Delta x$. The penalty constant in the Lax-Friedrichs numerical flux is chosen to be $\alpha_{LF} = 5$.

5 Numerical results

5.1 Test I: Deterministic Problem

We first examine the deterministic case, where (1) does not depend on the random variable z . We set the initial conditions as follows:

$$f_0(x, v) = \frac{e^{-v^2}}{\sqrt{\pi}}(1 + a_0 \sin(2\pi x)). \quad (43)$$

where $a_0 \in [0, 1]$ is a constant. We randomly generate 10 values for a_0 (assuming a uniform distribution). For each initial condition, we solve for reference solutions of the moments as described in 4.1. We then use all these reference moments up to time $t = 0.4$ as our training data. Once the network is properly trained, we test the performance of our model at time $t = 0.5$ with a new initial condition given by $a_0 = 0.9$. With this setup, we can analyze the generalizability of our model across different initial conditions and various time spots.

We compare the results with two constant choices for the collision frequency σ : $\sigma = 2$ and $\sigma = 10$, and three different number of moments N , including $N = 1$, $N = 3$ and $N = 5$. For $\sigma = 10$, in Figure 3, 4 and 5, we show the numerical solutions of m_0 and m_1 at $t = 0.5$ for $N = 1, 3, 5$, respectively. It can be observed that all closure models can achieve reasonably good approximation results with this large collision frequency. On the other hand, in Figure 6, 7 and 8, we show the numerical profile of m_0 and m_1 for smaller $\sigma = 2$ with $N = 1, 3, 5$ respectively. When $N = 5$ in Figure 8, there is no clear distinction between the prediction by different methods from the reference solution. When $N = 3$ in Figure 7, the errors for the P_N and LM model start to blow up, while those for the LG model are visible but insignificant compared to the other models, and the LG with hyperbolicity remain to be accurate. When $N = 1$ in Figure 6, even the solutions obtained by the LG model become oscillatory starting at $t = 0.4$. However, when the hyperbolic condition is added during the training process, the behavior of the solutions gets regulated and the model achieves a reasonable approximation to the benchmark solution obtained from the kinetic equation.

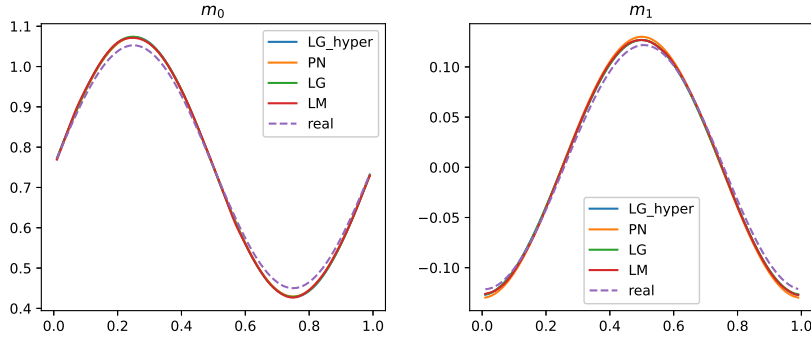


Fig. 3 Comparison between the benchmark results by solving kinetic equation (“real”) and predicted results using P_N model (“PN”), LM model (“LM”), LG model (“LG”) and LG model involving hyperbolicity (“LG_hyper”) with $N = 1$, $\sigma = 10$ at $t = 0.5$.

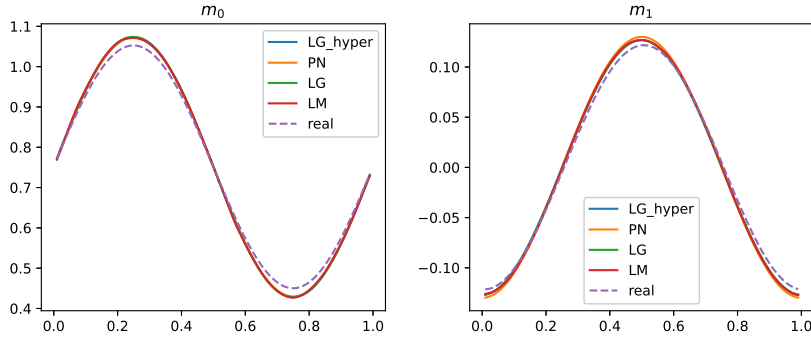


Fig. 4 Comparison between the benchmark results by solving kinetic equation (“real”) and predicted results using P_N model (“PN”), LM model (“LM”), LG model (“LG”) and LG model involving hyperbolicity (“LG_hyper”) with $N = 3$, $\sigma = 10$ at $t = 0.5$.

The reason for the incompetence of the LG model in the case $\sigma = 2$, $N = 1$ becomes apparent if we analyze the relative L^2 error when predicting $\partial_x m_{N+1}$ using neural networks. In Figure 2, we have demonstrated these errors for various N when $\sigma = 2$ and $\sigma = 10$. It can be clearly observed that when $\sigma = 2$, the predicting error for $N = 1$ is considerably more significant than that for $N = 3, 5$. This explains the large deviation from the reference solution when using LG method in this case. We can control the oscillation by adding hyperbolicity to our model, but the prediction of $\partial_x m_{N+1}$ still remains inaccurate, counting for the relatively large errors of the method LG_hyper in Figure 6. In contrast, when $\sigma = 10$, the predicting errors for $\partial_x m_{N+1}$ are much more

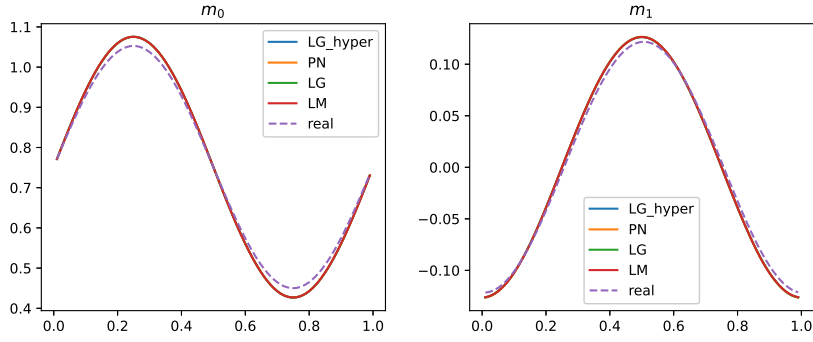


Fig. 5 Comparison between the benchmark results by solving kinetic equation (“real”) and predicted results using P_N model (“PN”), LM model (“LM”), LG model (“LG”) and LG model involving hyperbolicity (“LG_hyper”) with $N = 5$, $\sigma = 10$ at $t = 0.5$.

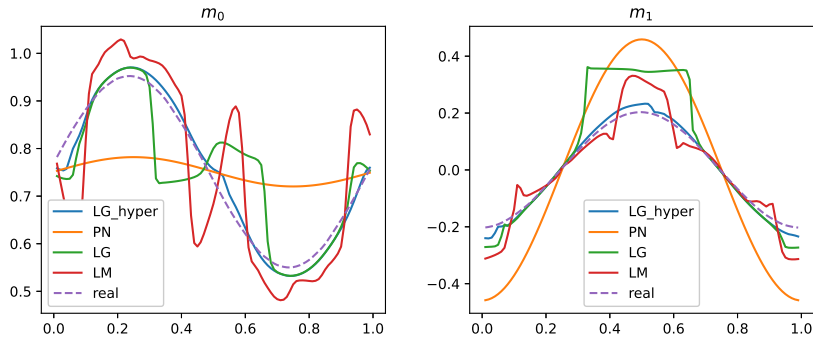


Fig. 6 Comparison between the benchmark results by solving kinetic equation (“real”) and predicted results using P_N model (“PN”), LM model (“LM”), LG model (“LG”) and LG model involving hyperbolicity (“LG_hyper”) with $N = 1$, $\sigma = 2$ at $t = 0.4$.

parallel among different choices of N , as shown in Figure 2. This explains why when $\sigma = 10$, the LG method performs well as N varies.

5.2 Test II: Random collision frequency

We now study the case with collision frequency σ involving randomness. We set $\sigma(z) = 2 + z$ where z follows the exponential distribution with parameter $\lambda = 1$, i.e., $\pi(z) = e^{-z}$ for $z \in [0, \infty)$. In this case, the gPC-basis functions

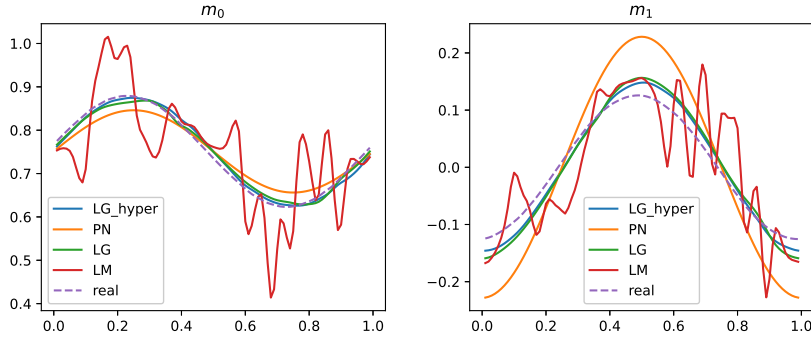


Fig. 7 Comparison between the benchmark results by solving kinetic equation (“real”) and predicted results using P_N model (“PN”), LM model (“LM”), LG model (“LG”) and LG model involving hyperbolicity (“LG_hyper”) with $N = 3$, $\sigma = 2$ at $t = 0.5$.

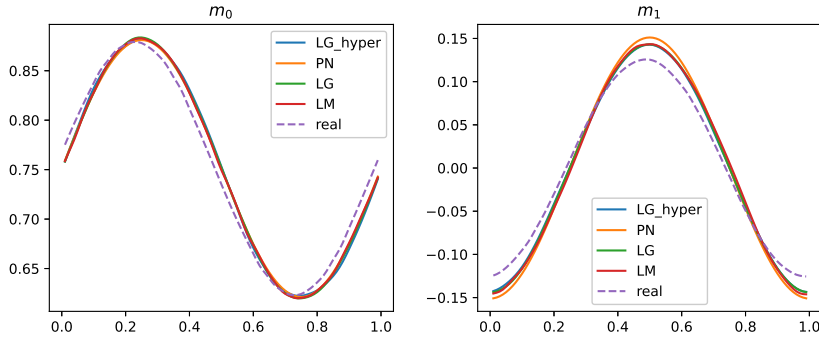


Fig. 8 Comparison between the benchmark results by solving kinetic equation (“real”) and predicted results using P_N model (“PN”), LM model (“LM”), LG model (“LG”) and LG model involving hyperbolicity (“LG_hyper”) with $N = 5$, $\sigma = 2$ at $t = 0.5$.

$\{\phi_i(z)\}_{i \geq 0}$ are given by the Laguerre polynomials with the recurrence relation:

$$\phi_{i+1}(z) = \frac{2i+1-z}{i+1} \phi_i(z) - \frac{i}{i+1} \phi_{i-1}(z), \quad i \geq 1, \quad (44)$$

and $\phi_0(z) = 1, \phi_1(z) = -z + 1$.

In Figure 9, we show the numerical simulation of the mean (m_0^0, m_1^0) of m_0 and m_1 with $N = 3$ at $t = 0.5$. In this example, the initial condition assumes the form of 43, with $a_0 = 0.9$. The training process is similar to that in the deterministic case, except that we replace the reference moments with their stochastic Galerkin counterparts. When performing the Galerkin expansion, we choose the order of truncation to be $K = 4$. One can observe that our

proposed LG model performs much better than the P_N model, especially when predicting the mean of m_1 .

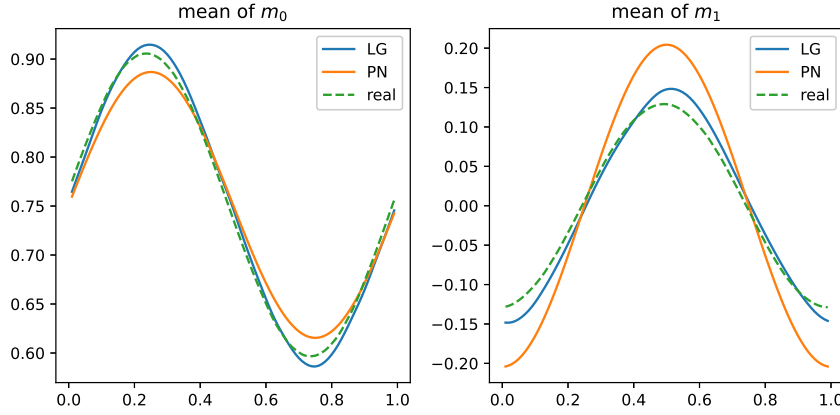


Fig. 9 Comparison of the mean (m_0^0, m_1^0) of m_0 and m_1 between the benchmark results by solving kinetic equation (“real”) and predicted results using P_N model (“PN”) and our proposed LG model (“LG”) for random collision frequency with $N = 3$ at $t = 0.5$.

5.3 Test III: Random initial data

In the following two tests, we consider the initial data containing uncertainties. The collision frequency is constant and set as $\sigma = 2$ in both tests below.

Test III (a): We study the problem with uncertain initial data, which is given by

$$f_0(x, v, z) = \frac{e^{-v^2}}{\sqrt{\pi}} (3 + (1 + z) \sin(2\pi x)), \quad (45)$$

where z follows the uniform distribution on $[-1, 1]$, i.e., $\pi(z) = \frac{1}{2}$ for $z \in I_z = [-1, 1]$. In this case, the gPC-basis functions $\{\phi_i(z)\}_{i \geq 0}$ are given by the Legendre polynomials in the recurrence relation:

$$\phi_{i+1}(z) = \frac{2i+1}{i+1} z \phi_i(z) - \frac{i}{i+1} \phi_{i-1}(z), \quad i \geq 1. \quad (46)$$

with $\phi_0(z) = 1, \phi_1(z) = z$. The basis functions are normalized in our simulation.

In Figure 10, we show the numerical solutions of the mean (m_0^0, m_1^0) of m_0 and m_1 with $N = 3$ at $t = 0.5$. We again set the order of truncation to be $K = 4$. Our proposed LG model accurately reproduces the mean of m_0 , while

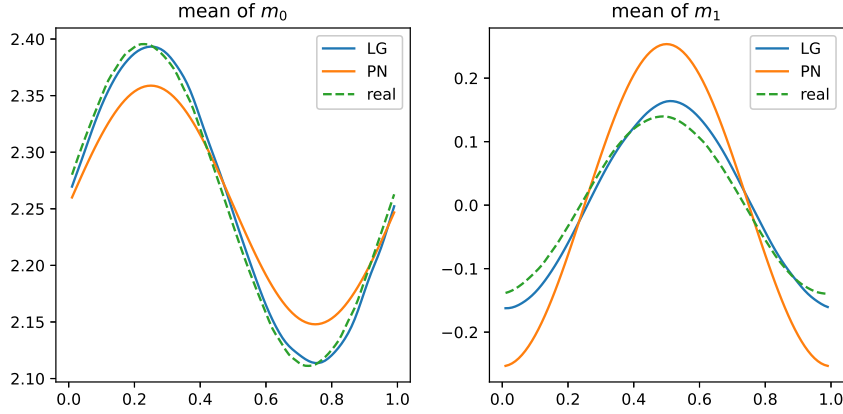


Fig. 10 Comparison of the mean (m_0^0, m_1^0) of m_0 and m_1 between the benchmark results by solving kinetic equation (“real”) and predicted results using P_N model (“PN”) and our proposed LG model (“LG”) for random initial data (45) with $N = 3$ at $t = 0.5$.

the error in the mean of m_1 is noticeable but significantly smaller compared to that in the P_N model.

Test III (b): In the last example, we assume the initial data contains uncertainty and is given as

$$f_0(x, v, z) = \frac{e^{-v^2}}{\sqrt{\pi}} (2 + \sin(2\pi x(1 + z))), \quad (47)$$

The setting for the random variable z and the choices of gPC basis functions as well as the truncation order are the same as in Test III (a) above.

Figure 11 illustrates the comparison for the mean (m_0^0, m_1^0) approximated by the P_N model and our proposed LG model. The P_N model exhibits significant errors in solving the system, whereas the LG model effectively captures the random effects, even as the true solutions exhibit more oscillatory behavior compared to the previous test. The deviation in the LG model, particularly for m_1 , becomes noticeable; however, the errors remain substantially smaller than those observed in the P_N model.

6 Conclusion

In this work, we develop a machine learning (ML)-based moment closure model for the linear Boltzmann equation in semiconductor devices, addressing both deterministic and stochastic settings. By using neural networks to approximate the spatial gradient of the unclosed highest-order moment, our approach achieves effective training to close the moment system. To guarantee its global hyperbolicity and stability, we imposed constraints for ensuring the symmetrizable hyperbolicity. For the stochastic problem, we incorporated a gPC-based

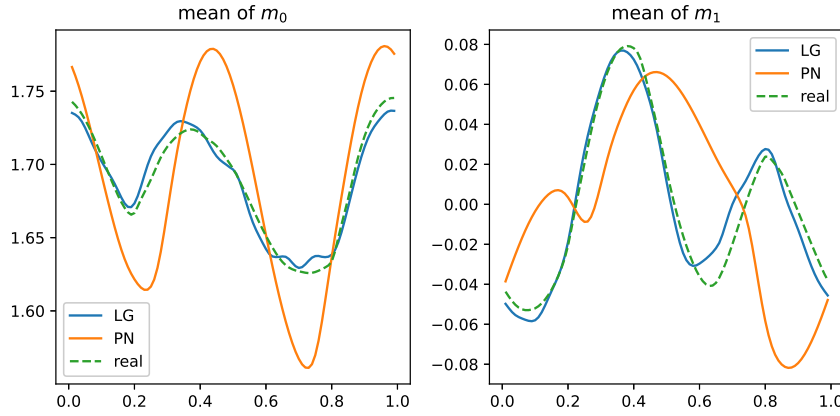


Fig. 11 Comparison of the mean (m_0^0, m_1^0) of m_0 and m_1 between the benchmark results by solving kinetic equation (“real”) and predicted results using P_N model (“PN”) and our proposed LG model (“LG”) for random initial data (47) with $N = 3$ at $t = 0.5$.

SG method to discretize the random variables, transforming the problem into one that is similar to the deterministic setting. Several numerical experiments validate the proposed framework, highlighting its stability and accuracy in achieving reliable moment closures for linear transport problems with (or without) uncertainties. These results underscore the potential of incorporating ML techniques to the moment closure of the more complicated nonlinear Boltzmann equation in our future work.

References

1. Albi, G., Herty, M., Pareschi, L.: Kinetic description of optimal control problems and applications to opinion consensus. *Commun. Math. Sci.* **13**(6), 1407–1429 (2015)
2. Alldredge, G.W., Frank, M., Hauck, C.D.: A regularized entropy-based moment method for kinetic equations. *SIAM J. Appl. Math.* **79**(5), 1627–1653 (2019)
3. Alonso, R.: Boltzmann-type equations and their applications. *Publicações Matemáticas do IMPA*. [IMPA Mathematical Publications]. Instituto Nacional de Matemática Pura e Aplicada (IMPA), Rio de Janeiro (2015). 30o Colóquio Brasileiro de Matemática. [30th Brazilian Mathematics Colloquium]
4. Ansgar, J.: Transport equations for semiconductors. *Lecture Notes in Physics* **773** (2009)
5. Bois, L., Franck, E., Navoret, L., Vigon, V.: A neural network closure for the Euler-Poisson system based on kinetic simulations. *Kinet. Relat. Models* **15**(1), 49–89 (2022)
6. Brunton, S.L., Proctor, J.L., Kutz, J.N.: Discovering governing equations from data by sparse identification of nonlinear dynamical systems. *Proc. Natl. Acad. Sci. USA* **113**(15), 3932–3937 (2016)
7. Caffisch, R., Silantyev, D., Yang, Y.: Adjoint DSMC for nonlinear Boltzmann equation constrained optimization. *J. Comput. Phys.* **439**, Paper No. 110404, 29 (2021)
8. Cai, Z., Fan, Y., Li, R.: Globally hyperbolic regularization of Grad’s moment system in one dimensional space. *Commun. Math. Sci.* **11**(2), 547–571 (2013)

9. Cai, Z., Fan, Y., Li, R.: Globally hyperbolic regularization of Grad's moment system. *Comm. Pure Appl. Math.* **67**(3), 464–518 (2014)
10. Cai, Z., Fan, Y., Li, R.: On hyperbolicity of 13-moment system. *Kinet. Relat. Models* **7**(3), 415–432 (2014)
11. Cai, Z., Fan, Y., Li, R.: Hyperbolic model reduction for kinetic equations. In: *Recent advances in industrial and applied mathematics, ICIAM 2019 SEMA SIMAI Springer Ser.*, vol. 1, pp. 137–157. Springer, Cham (2022)
12. Cai, Z., Li, R.: Numerical regularized moment method of arbitrary order for Boltzmann-BGK equation. *SIAM J. Sci. Comput.* **32**(5), 2875–2907 (2010)
13. Caponigro, M., Fornasier, M., Piccoli, B., Trélat, E.: Sparse stabilization and optimal control of the Cucker-Smale model. *Math. Control Relat. Fields* **3**(4), 447–466 (2013)
14. Chandrasekhar, S.: On the radiative equilibrium of a stellar atmosphere. *Astrophys. J.* **99**, 180–190 (1944)
15. Cheng, Y., Gamba, I.M., Ren, K.: Recovering doping profiles in semiconductor devices with the Boltzmann-Poisson model. *J. Comput. Phys.* **230**(9), 3391–3412 (2011)
16. Choulli, M., Stefanov, P.: Inverse scattering and inverse boundary value problems for the linear Boltzmann equation. *Comm. Partial Differential Equations* **21**(5-6), 763–785 (1996)
17. Christlieb, A.J., Ding, M., Huang, J., Krupansky, N.A.: Hyperbolic machine learning moment closures for the BGK equations. *arXiv preprint arXiv:2401.04783* (2024)
18. Daus, E.S., Jin, S., Liu, L.: Spectral convergence of the stochastic Galerkin approximation to the Boltzmann equation with multiple scales and large random perturbation in the collision kernel. *Kinet. Relat. Models* **12**(4), 909–922 (2019)
19. Dimarco, G., Pareschi, L.: Numerical methods for kinetic equations. *Acta Numer.* **23**, 369–520 (2014)
20. Fan, Y., Li, R., Zheng, L.: A nonlinear hyperbolic model for radiative transfer equation in slab geometry. *SIAM J. Appl. Math.* **80**(6), 2388–2419 (2020)
21. Fan, Y., Li, R., Zheng, L.: A nonlinear moment model for radiative transfer equation in slab geometry. *J. Comput. Phys.* **404**, 109128, 23 (2020)
22. Grad, H.: On the kinetic theory of rarefied gases. *Comm. Pure Appl. Math.* **2**, 331–407 (1949)
23. Grad, H.: Principles of the kinetic theory of gases. *Handbuch der Physik [Encyclopedia of Physics]*, Bd. 12, *Thermodynamik der.* Springer-Verlag, Berlin-Göttingen-Heidelberg (1958). Herausgegeben von S. Flügge
24. Han, J., Jentzen, A., E, W.: Solving high-dimensional partial differential equations using deep learning. *Proc. Natl. Acad. Sci. USA* **115**(34), 8505–8510 (2018)
25. Han, J., Ma, C., Ma, Z., E, W.: Uniformly accurate machine learning-based hydrodynamic models for kinetic equations. *Proc. Natl. Acad. Sci. USA* **116**(44), 21983–21991 (2019)
26. Hauck, C.D., McClarren, R.: Positive P_N closures. *SIAM J. Sci. Comput.* **32**(5), 2603–2626 (2010)
27. Hu, J., Jin, S.: A stochastic Galerkin method for the Boltzmann equation with uncertainty. *J. Comput. Phys.* **315**, 150–168 (2016)
28. Hu, J., Pareschi, L., Wang, Y.: Uncertainty quantification for the BGK model of the Boltzmann equation using multilevel variance reduced Monte Carlo methods. *SIAM/ASA J. Uncertain. Quantif.* **9**(2), 650–680 (2021)
29. Hu, J., Qi, K.: A fast Fourier spectral method for the homogeneous Boltzmann equation with non-cutoff collision kernels. *J. Comput. Phys.* **423**, 109806, 21 (2020)
30. Hu, J., Qi, K., Yang, T.: A new stability and convergence proof of the Fourier-Galerkin spectral method for the spatially homogeneous Boltzmann equation. *SIAM J. Numer. Anal.* **59**(2), 613–633 (2021)
31. Huang, J., Cheng, Y., Christlieb, A.J., Roberts, L.F.: Machine learning moment closure models for the radiative transfer equation I: directly learning a gradient based closure. *J. Comput. Phys.* **453**, Paper No. 110941, 21 (2022)
32. Huang, J., Cheng, Y., Christlieb, A.J., Roberts, L.F.: Machine learning moment closure models for the radiative transfer equation III: Enforcing hyperbolicity and physical characteristic speeds. *J. Sci. Comput.* **94**(1), Paper No. 7, 27 (2023)

33. Huang, J., Cheng, Y., Christlieb, A.J., Roberts, L.F., Yong, W.A.: Machine learning moment closure models for the radiative transfer equation II: enforcing global hyperbolicity in gradient-based closures. *Multiscale Model. Simul.* **21**(2), 489–512 (2023)
34. Huang, J., Ma, Z., Zhou, Y., Yong, W.A.: Learning thermodynamically stable and galilean invariant partial differential equations for non-equilibrium flows. *Journal of Non-Equilibrium Thermodynamics* **46**(4), 355–370 (2021)
35. Jiang, G.S., Shu, C.W.: Efficient implementation of weighted ENO schemes. *J. Comput. Phys.* **126**(1), 202–228 (1996)
36. Jin, S.: Mathematical analysis and numerical methods for multiscale kinetic equations with uncertainties. In: *Proceedings of the International Congress of Mathematicians—Rio de Janeiro 2018. Vol. IV. Invited lectures*, pp. 3611–3639. World Sci. Publ., Hackensack, NJ (2018)
37. Jin, S., Pareschi, L. (eds.): *Uncertainty quantification for hyperbolic and kinetic equations, SEMA-SIMAI Springer Series*, vol. 14. Springer (2017)
38. Jin, S., Xiu, D., Zhu, X.: Asymptotic-preserving methods for hyperbolic and transport equations with random inputs and diffusive scalings. *J. Comput. Phys.* **289**, 35–52 (2015)
39. Levermore, C.D.: Moment closure hierarchies for kinetic theories. *J. Statist. Phys.* **83**(5-6), 1021–1065 (1996)
40. Li, Q., Wang, L.: Uniform regularity for linear kinetic equations with random input based on hypocoercivity. *SIAM/ASA J. Uncertain. Quantif.* **5**(1), 1193–1219 (2017)
41. Li, R., Li, W., Zheng, L.: Direct flux gradient approximation to moment closure of kinetic equations. *SIAM J. Appl. Math.* **81**(5), 2153–2179 (2021)
42. Liu, L., Jin, S.: Hypocoercivity based sensitivity analysis and spectral convergence of the stochastic Galerkin approximation to collisional kinetic equations with multiple scales and random inputs. *Multiscale Model. Simul.* **16**(3), 1085–1114 (2018)
43. Liu, L., Qi, K.: Convergence of the fourier-galerkin spectral method for the boltzmann equation with uncertainties. *Commun. Math. Sci.* **22**(7), 1897–1925 (2024)
44. Liu, L., Qi, K.: Spectral convergence of a semi-discretized numerical system for the spatially homogeneous boltzmann equation with uncertainties. *SIAM/ASA J. Uncertain. Quantif.* **12**(3), 812–841 (2024)
45. Ma, C., Zhu, B., Xu, X.Q., Wang, W.: Machine learning surrogate models for landau fluid closure. *Physics of Plasmas* **27**(4) (2020)
46. Markowich, P.A., Ringhofer, C.A., Schmeiser, C.: *Semiconductor equations*. Springer-Verlag, Vienna (1990)
47. McClarren, R.G., Hauck, C.D.: Robust and accurate filtered spherical harmonics expansions for radiative transfer. *J. Comput. Phys.* **229**(16), 5597–5614 (2010)
48. Mouhot, C., Pareschi, L.: Fast algorithms for computing the Boltzmann collision operator. *Math. Comp.* **75**, 1833–1852 (2006)
49. Mouhot, C., Pareschi, L., Rey, T.: Convolutional decomposition and fast summation methods for discrete-velocity approximations of the Boltzmann equation. *ESAIM: Math. Model. Numer. Anal. (M2AN)* **47**, 1515–1531 (2013)
50. Pareschi, L.: An introduction to uncertainty quantification for kinetic equations and related problems. In: *Trails in kinetic theory, SEMA SIMAI Springer Ser.*, vol. 25, pp. 141–181. Springer, Cham (2021)
51. Pareschi, L., Zanella, M.: Monte Carlo stochastic Galerkin methods for the Boltzmann equation with uncertainties: Space-homogeneous case. *Journal of Computational Physics* p. 423:109822 (2020)
52. Poëtte, G.: A gPC-intrusive Monte-Carlo scheme for the resolution of the uncertain linear Boltzmann equation. *J. Comput. Phys.* **385**, 135–162 (2019)
53. Radice, D., Abdikamalov, E., Rezzolla, L., Ott, C.D.: A new spherical harmonics scheme for multi-dimensional radiation transport I. Static matter configurations. *J. Comput. Phys.* **242**, 648–669 (2013)
54. Scoggins, J.B., Han, J., Massot, M.: Machine learning moment closures for accurate and efficient simulation of polydisperse evaporating sprays. In: *AIAA Scitech 2021 Forum*, p. 1786 (2021)
55. Serre, D.: *Systems of conservation laws. 1*. Cambridge University Press, Cambridge (1999). *Hyperbolicity, entropies, shock waves*, Translated from the 1996 French original by I. N. Sneddon

56. Shu, C.W., Osher, S.: Efficient implementation of essentially non-oscillatory shock-capturing schemes. *Journal of computational physics* **77**(2), 439–471 (1988)
57. Struchtrup, H., Torrillon, M.: Regularization of grad’s 13 moment equations: Derivation and linear analysis. *Phys. Fluids* **15**(9), 2668–2680 (2003)
58. Taheri, P., Torrillon, M., Struchtrup, H.: Couette and poiseuille microflows: Analytical solutions for regularized 13-moment equations. *Phys. Fluids* **21:017102** (2009)
59. Torrillon, M.: Modeling nonequilibrium gas flow based on moment equations. In: Annual review of fluid mechanics. Vol. 48, *Annu. Rev. Fluid Mech.*, vol. 48, pp. 429–458. Annual Reviews, Palo Alto, CA (2016)
60. Villani, C.: A review of mathematical topics in collisional kinetic theory. In: S. Friedlander, D. Serre (eds.) *Handbook of Mathematical Fluid Mechanics*, vol. I, pp. 71–305. North-Holland (2002)
61. Wang, L., Xu, X.Q., Zhu, B., Ma, C., Lei, Y.A.: Deep learning surrogate model for kinetic landau-fluid closure with collision. *AIP Advances* **10**(7) (2020)
62. Xiu, D.: *Numerical Methods for Stochastic Computations*. Princeton University Press, New Jersey (2010)